SIMULTANEOUS MEASUREMENT OF q AND E$_r$ PROFILES USING THE MOTIONAL STARK EFFECT IN HIGH-PERFORMANCE DIII–D PLASMAS

by

B.W. RICE, K.H. BURRELL, L.L. LAO, and D.G. NILSON*

JULY 1998

DISCLAIMER

SIMULTANEOUS MEASUREMENT OF q AND E$_r$ PROFILES USING THE MOTIONAL STARK EFFECT IN HIGH-PERFORMANCE DIII–D PLASMAS

by

B.W. RICE,* K.H. BURRELL, L.L. LAO, and D.G. NILSON*

*Lawrence Livermore National Laboratory

Simultaneous Measurement of q and E_r Profiles Using the Motional Stark Effect in High-Performance DIII-D Plasmas

B. W. Rice,[a)] K.H. Burrell, L.L. Lao, D.G. Nilson[a(]

General Atomics, P.O. Box 85608, San Diego, California 92186-5608

(November 24, 1998)

Abstract

The Motional Stark Effect (MSE) diagnostic was developed to provide a measurement of the magnetic pitch angle or q profile in tokamaks. The technique relies upon polarization measurements of Stark broadened D_α emission to determine the pitch angle of the Lorentz $v_b \times B$ electric field, where v_b is the injected neutral beam particle velocity and B is the total magnetic field. However, in many advanced confinement regimes, large values of the plasma radial electric field, E_r, are observed and can affect the interpretation of MSE measurements. Viewing fixed locations in the plasma from two different viewing angles allows one to separate the E_r field from the $v_b \times B$ field, thus providing simultaneous measurement of the E_r and q profiles. To achieve this measurement, the DIII-D MSE diagnostic was recently upgraded from 16 to 35 channels with three independent viewing angles. The new instrument provides an E_r resolution of 10 kV/m with a time response of 1 ms. Measurement results from VH-mode, reverse shear, and H-mode plasmas are presented.

I. INTRODUCTION

The Motional Stark Effect (MSE) diagnostic has developed into a reliable and routine instrument for measurement of the current density (J) profile in tokamaks equipped with

neutral beams. First demonstrated on PBX-M [1], and shortly after on DIII-D [2], MSE is now in use or being developed on most of the world's major tokamaks. The MSE diagnostic provides a measurement of the local magnetic field pitch angle B_{pol}/B_T, and when used as input to an equilibrium reconstruction code, these measurements provide a simple and direct constraint on the $J(\rho)$ or safety factor $q(\rho)$ profile. Access to high quality q profile measurements has led to advancements in the understanding of stability and confinement in tokamak plasmas. The most recent example is the development of improved confinement regimes in discharges with negative central magnetic shear (NCS) [3–5].

In many of these advanced regimes with improved confinement, a large radial electric field, E_r, is observed. Indeed, the combination of favorable magnetic shear for MHD stability coupled with $E \times B$ shear stabilization of turbulence is the leading model for explaining the improved confinement in many regimes including H-mode and NCS [6]. It was recognized recently that large values of E_r can significantly effect the interpretation of MSE measurements of the q profile [7,8]. It was also shown that with additional MSE measurements, one can extract a direct measurement of E_r in addition to the usual magnetic field pitch measurement. In recent work on DIII-D, 19 additional MSE channels with new viewing angles were added to the existing system (for a total of 35 channels) in order to resolve the E_r field [9]. In this paper, the new MSE system is described and data illustrating the simultaneous measurement of the q and E_r profiles are presented. We show that the E_r effect does change our interpretation of the q profile and that the direct MSE measurement of E_r is in good agreement with the value calculated from charge-exchange recombination (CER) measurements. Measurements from high-performance VH-mode and NCS plasmas, and to E_r well measurements at the edge of H-mode plasmas, are presented. The impact of E_r on sawtooth measurements is also discussed.

The emphasis in this paper is primarily on the E_r aspect of the MSE measurement. For more general background information on the MSE diagnostic the reader is referred to earlier publications [1,2,10,11].

II. EFFECT OF E_R ON MSE PITCH ANGLE

The MSE measurement relies upon the splitting of the Balmer-α line into orthogonally polarized components (σ,π) as a result of the strong electric field in the rest frame of deuterium atoms injected by a high-energy neutral beam [1,2]. When viewed in a direction perpendicular to $\mathbf{E}$, the Stark components σ and π are polarized perpendicular and parallel to $\mathbf{E}$, respectively. The total electric field in the rest frame of the neutral beam atoms traveling with velocity v_b is the sum of the Lorentz $\mathbf{E_b} = \mathbf{v_b} \times \mathbf{B}$ field and the plasma radial electric field E_r. E_r results from radial force balance in the plasma and is given by

$$E_r = (Z_i e n_i)^{-1} \nabla P_i - v_{\theta i} B_\phi + v_{\phi i} B_\theta, \tag{1}$$

where Z_i is the ion charge, n_i is the ion density, e is the electronic charge, P_i is the ion pressure, $v_{\theta i}$, $v_{\phi i}$ are the poloidal and toroidal fluid rotation velocities, and B_θ, B_ϕ are poloidal and toroidal fields. This equation is valid for both the main ion and impurity species. The direction of E_r is perpendicular to the flux surface.

The electric field vectors at the torus midplane are shown in Fig. 1. It is important to note that while the large $v_b \times B_T$ field (out of the page) provides most of the Stark broadening, the E_r vector adds to the smaller $v_b \times B_{pol}$ field, thus the relative importance of E_r is larger than might be expected. The relationship between the polarization angle of the Stark σ component and the magnetic field and E_r components has been derived previously [7]. Using the viewing geometry shown in Fig. 1, the polarization angle of the electric field is given by

$$\tan\gamma = \frac{A_1 B_z + A_5 E_R}{A_2 B_\phi + A_3 B_R + A_4 B_Z + A_6 E_Z + A_7 E_R} \tag{2}$$

where R is the major radius and Z is in the vertical direction. The A coefficients are viewing geometry dependent terms given by

$$A_1 = -\cos(\alpha + \Omega)$$

$$A_2 = \sin\alpha \cos\theta$$

$$A_3 = \cos\alpha \cos\theta$$

$$A_4 = \sin(\alpha + \Omega)\sin\theta$$

$$A_5 = -\cos(\Omega)/v_b$$

$$A_6 = -\cos\theta/v_b$$

$$A_7 = \sin\theta \sin\Omega/v_b$$

where θ is a small tilt angle out of the horizontal plane. On DIII-D, the quantities B_R, E_Z, and θ are small near the midplane giving an approximate relation

$$\tan\gamma \approx \frac{A_1 B_z + A_5 E_R}{A_2 B_\phi} \quad . \tag{3}$$

Since coefficients A_1 and A_5 vary differently depending on viewing geometry and beam velocity, we see that with two MSE systems viewing the same radial location in the plasma but with different A_i coefficients, one can determine both the poloidal field (B_Z at the midplane) and the E_R field. Using Eq. 3 and defining an effective measured vertical field as $B_{Z0} \equiv (A_2/A_1)B_\phi \tan\gamma$ (i.e. the measured vertical field assuming E_R=0), then E_r at a radius R is given by

$$E_R \approx \frac{A_1 A_1'(B_{Z0} - B_{Z0}')}{A_5 A_1' - A_1 A_5'} \quad . \tag{4}$$

where the primed terms refer to a second MSE system view the same radial location but with different A_i coefficients.

III. INSTRUMENT DESIGN

Viewing the full and half beam energy Stark components is one option for obtaining different A_i coefficients, but this technique suffers from poor plasma penetration of the half energy component and the fact that the velocities differ by only $\sqrt{2}$. Instead, on DIII-D, we opted to add nineteen additional channels (mostly radial) as indicated by the dashed lines-of-sight in Fig. 2, providing two different viewing angles across most of the plasma. The variation in the A_5 coefficient and the radial resolution is shown in Fig. 3. The A_5 coefficient is near zero for the radial channels, thus the tangential chords are most sensitive

to E_r. Because of the finite beam width of 14 cm, the new radial channels have worse spatial resolution ($\delta R \sim$ 13 - 23 cm) than the tangential channels ($\delta R \sim$1.5 - 5 cm). This compromise was necessary given the DIII-D geometry which has only co-directed beams. Note that a MSE system viewing both a co- and counter-directed beam would achieve maximum E_r resolution with the optimum radial resolution.

The hardware design for the new channels (Fig. 4) essentially duplicates that of the edge viewing MSE system at the 45 degree port [11] except that no reflector is necessary. Light is collected through a series of 3 lenses constructed of low Verdet constant glass (Schott SFL6) to minimize Faraday rotation effects. A shutter with in-vacuum polarizers is provided to protect the optics during glow discharge cleaning; the polarizer is used for calibration and debugging the instrument. Following the lenses, light is focussed through dual photoelastic modulators (PEM) operating at 20 and 23 kHz, and a sheet polarizer. An array of 6 vertically stacked 1 mm fibers relay the light to a remote diagnostic lab for detection. The lenses provide a magnification of approximately 10, resulting in a plasma spot size that is about 1 cm wide by 7 cm high. In the diagnostic lab, the fiber output is expanded and collimated to pass through interference filters with a 3 Angstrom bandwidth. Each filter can be rotated through small angles to provided fine tuning of the central wavelength. The signal is then detected using photomultiplier tubes and lock-in amplifiers referenced to the 2nd harmonic of the PEM modulation frequency.

IV. EQUILIBRIUM RECONSTRUCTION

It is possible to obtain an approximate estimate of E_r without an equilibrium reconstruction by using Eq. 4 directly. This type of analysis would be suitable for a feedback system to do real-time control of the E_r profile. However, for more accurate analysis, especially in shaped plasmas, we require a full equilibrium reconstruction that self-consistently solves for both the q and E_r profiles for a given set of MSE data. On DIII-D this is done using the EFIT equilibrium reconstruction code [12]. Since EFIT utilizes a flux surface geometry, and

E_r is not constant on a flux surface, we instead use the gradient of the electrostatic potential Φ, which is a flux surface quantity. The relationship between E_r and Φ is given by

$$\mathbf{E_r} = -\nabla\Phi = -\frac{\partial\Phi}{\partial\psi}\nabla\psi \qquad (5)$$

$$= -\omega R B_R \hat{Z} + \omega R B_Z \hat{R} \qquad (6)$$

where ψ is the poloidal flux and we have introduced the definition $\omega \equiv \partial\Phi/\partial\psi$, which has dimensions of frequency. Either a polynomial or spline representation can be used for $\omega(\psi)$ in addition to the usual flux functions $p'(\psi)$ and $ff'(\psi)$ in the Grad-Shafranov equation. The components B_Z, B_R, and B_ϕ are calculated from ψ and E_R, E_Z are calculated from Eq. (5); this allows $\tan\gamma$ to calculated from Eq. (2) for use in the χ^2 minimization procedure. The fitting parameters for ω, p', and ff' are adjusted to minimize χ^2 on external magnetics, internal MSE measurements, and optionally pressure profile data.

V. E_R PROFILE MEASUREMENTS

A. Advanced Tokamak Modes

The shape of the E_r profile and its affect on the q profile measurement can vary widely depending on the confinement regime. In this section, we will present data from two advanced confinement regimes on DIII-D where the E_r field is significant. These include ELM-free VH-mode and NCS with and internal transport barrier and an L-mode edge. Unless otherwise noted, all discharges shown in this section were formed with deuterium fuel at a toroidal field of 2.1 T.

The time evolution for a 1.6 MA VH-mode discharge is given in Fig. 5. This discharge has a confinement enhancement relative to the ITER89P scaling of $H = 3.5$ and normalized beta of $\beta_N = 3.6$ (% T m/MA), typical of VH-mode plasmas. The ELM-free period is shorter than usual because the shape is upper single null instead of the more typical double null configuration. In Fig. 5(c), the effective vertical field B_{Z0} (assuming $E_r = 0$) is plotted for a tangential chord (solid line) and a radial chord (dashed line) at a radius of $R = 2$ m.

6

If E_r were zero, then these two curves would track one another. The separation of the two curves during the ELM-free period from 2–2.25 s is an indication of the buildup of radial electric field. Using Eq. (4), the radial electric field at $R = 2$ m is calculated directly from the MSE measurements as shown in Fig. 5(d). The time evolution of E_r follows closely the time evolution of the plasma toroidal rotation in Fig. 5(e) obtained from charge-exchange recombination (CER) [13] measurements of carbon impurities. As is typical of most VH-mode discharges in DIII-D, E_r in Eq. 1 is dominated by the strong toroidal rotation term due to tangentially directed beams on DIII-D. The maximum time response of the MSE E_r measurement is 1 ms with an RMS noise resolution of 7 kV/m. The curve in Fig.5(c) was generated using a 5 ms sliding boxcar average giving somewhat better resolution. Depending on discharge conditions, systematic errors in E_r due to spatial averaging in the radial chords and calibration are a factor of 2–3 larger than uncertainties due to noise at present. An additional point-of-interest in this discharge is that a locked-mode develops after the collapse in β from 2.5–3 s. During this time the impurity rotation shows a small negative rotation. In agreement with this observation, the MSE radial electric field measurement also reverses sign during mode-locking.

To determine the profile of E_r, we first look at the profiles B_{Z0} shown in Fig. 6. At 1.625 s, during the low-power L-mode portion of the discharge, the effective vertical field calculated from both the tangential (circles) and radial (diamonds) systems agree, indicating almost unmeasurable levels of E_r. However, by 2.2 s the tangential and radial profiles have significantly deviated from one another indicating large E_r. This figure illustrates how large the effect of E_r can be on the interpretation of the poloidal field. The radial channels, with $A_5 \sim 0$ more closely represent the actual poloidal field, while the tangential channels show a different slope due to the E_r contribution.

Using the EFIT equilibrium reconstruction method described earlier, a self-consistent fit to the E_r and q profiles at 2.2 s are obtained as shown by the solid curves in Figure 7. In this case a two term polynomial fit was used for ω. Since E_r is a relatively smooth function, no improvement in χ^2 was obtained by adding additional polynomial terms to the ω function.

For comparison, the dashed line indicates the CER measurement of E_r obtained from Eq. (1). The agreement between the two instruments is better than 20 kV/m over the entire plasma radius.

In addition to providing a direct local measurement of E_r, the new MSE measurements also allow the q profile to be calculated with improved accuracy. The dashed curve in Fig. 7a shows the q profile that results when only the tangential MSE chords are used and E_r is assumed to be zero. The difference in q_0 is quite large, especially during the high-performance ELM-free period. Such changes would have an important effect on stability calculations.

NCS discharges have a decidedly different E_r profile shape compared with VH-mode. These discharges are formed by injecting neutral beam power during the current ramp [14] to slow the diffusion of current allowing a skin current to form. With sufficient injected power, a core transport barrier will generally form leading to peaked ion temperature, toroidal rotation, and in many cases density profiles. A very strong NCS discharge with 7.5 MW of beam power during the current ramp is shown in Fig. 8, including EFIT reconstruction of E_r and q profiles, and the CER profiles T_i, rotation, and E_r. The agreement between MSE and CER measurements of E_r is reasonably good in the core, but there is some disagreement in the range of 2.-2.1 m. While the overall profile of E_r indicates again that it is dominated by toroidal rotation, the steep gradient in E_r near $R = 2$ m results from the strong negative E_r contribution due to a large p'. It is not completely clear yet whether the strong shear in E_r at 2 m is the cause or consequence of the large resulting pressure gradient. Note that in the outer region of the plasma, which remains in a turbulent L-mode confinement state, E_r and shear in $E \times B$ remain small.

B. Edge E_r Well Measurements in H-mode Plasmas

After the edge viewing MSE system was installed on DIII-D in 1995 [11], large perturbations in the pitch angle profile have frequently been observed within a few centimeters of the

separatix in H-mode discharges. At first, it was thought that the perturbation represented bootstrap current due to the steep pressure gradient at the edge. However, equilibrium reconstructions indicated that the perturbation was too large to be a physically acceptable current. It is now clear that the edge perturbation represents the E_r well associated with H-mode.

Unfortunately it was not possible to construct multiple MSE views of the edge with good spatial resolution due to viewing port constraints. There is another approach, however, that gives good results. Assuming that the poloidal field at the plasma edge is fairly well constrained by EFIT using the extensive external magnetic loop measurements, then E_r can be determined from the tangential MSE channels viewing from the 45 degree port. As part of the E_r upgrade, an additional channel was added to the edge region, giving a channel spacing of 2.2 cm and a spatial resolution (spot size) of ~ 1 cm. Because of the very narrow width of the edge E_r well, the 2.2 cm channel spacing is still not adequate to resolve the E_r well in detail. To improve this situation, we performed outer separatrix sweeps of 3-8 cm to map out the E_r well in more detail. To analyze this data, a series of EFIT reconstructions were performed during the sweep, providing a time history of the edge magnetic field components and separatrix location. For each time slice, the MSE radial locations are mapped to a normalized radius ρ, then for one time during the sweep all data is mapped from ρ back to major radius. E_r data is constructed by solving Eq. 2 for E_r using the B components from EFIT and assuming $E_Z = 0$ at the midplane.

The resulting data is shown in Fig. 9 for discharges with an L-mode, ELM-free VH-mode, and ELMing H-mode edge. The L-mode and ELM-free discharges have triangularity $\delta \sim 0.8$ while the ELMing H-mode is lower single null with $\delta \sim 0.4$. For comparison, CER measurements of the E_r well are given in Fig. 9(b). CER measurements were not available for the ELM-free case in Fig. 9(c), so the comparison was made for a similar discharge without a sweep in Fig. 9(d). Qualitatively the agreement between the CER and MSE measurements is good, although the MSE data generally shows deeper and narrower wells than CER. The main systematic error in the CER system is spatial smearing on the vertical chords required

for poloidal rotation suffer due to the large height (~ 40 cm) of the DIII-D neutral beam. For MSE, the main uncertainty is accuracy in reconstructing the edge poloidal field.

Although measurements of the edge E_r well have been published previously [6], they are usually at the time around the L-H transition when the E_r well is just forming. The large depth and narrow width of the E_r well observed the later phases of ELM-free discharges like Fig. 9(c) has not been reported previously. The peak shearing rate in this region is very large, reaching a maximum of 3×10^6 s^{-1}. The large shear results from strong toroidal rotation inside $R = 2.26$ cm giving a large positive E_r value, coupled with strong pressure gradient and poloidal rotation terms that drive E_r negative just inside the separatrix.

VI. EFFECT OF E_R ON Q_0 DURING SAWTEETH

Finally, we comment on the effect of E_r during sawteeth measurements. Despite the improvement in q profile diagnostics that has taken place in the last 10 years, there is still considerable debate over the evolution of the q profile during sawteeth. Some measurements show q_0 remaining below one (~ 0.7) during sawteeth indicating that the complete reconnection does not occur. Other measurements show q_0 closer to one, consistent with the Kadomtsev reconnection model. On DIII-D, MSE measurements have always shown q_0 close to one, dropping to ~ 0.9-0.95 before a sawtooth crash and returning to near unity after the crash. An important question is whether including E_r in the MSE analysis significantly change these results. Because the $m/n = 1/1$ instability associated with sawteeth restricts the toroidal rotation to fairly small values, generally < 50 km/sec, E_r is quite small in the core and the effect on the EFIT reconstruction of q_0 is minor. Shown in Fig. 10 is the value of q_0 for a sawtoothing discharge calculated using the tangential MSE channels and assuming $E_r = 0$ (dashed), versus q_0 calculated from the full MSE system including E_r. The E_r corrected q_0 evolution remains consistent with the previous DIII-D result of complete reconnection after the sawtooth crash.

VII. CONCLUSION

It has been demonstrated on DIII-D that multiple viewing MSE systems can provide simultaneous measurements of the q and E_r profiles. The statistical uncertainty in E_r is ~ 7 kV/m with a time response of 1 ms. While the uncertainty due to statistical fluctuations can be reduced with time averaging, systematic errors due to spatial averaging or offset calibration may be larger depending on plasma conditions. E_r profiles calculated independently from CER and MSE measurements are in good agreement within experimental uncertainties. We note that CER analysis of the E_r profile is a very manpower intensive task, while the MSE measurements can be obtained almost immediately after a discharge. A real-time measurement of local E_r suitable for feedback control of the $\mathbf{E_r} \times \mathbf{B}$ velocity shear can be obtained directly from MSE data using Eq. (4). Future MSE upgrades under consideration include accounting for spatial averaging in EFIT, installing a counter beam to improve spatial resolution, and increasing the number of edge chords for improved E_r well and edge J measurements.

VIII. ACKNOWLEDGMENT

REFERENCES

[1] F.M. Levinton, *et al.*, Phys. Rev. Lett. **63**, 2060 (1989).

[2] D. Wroblewski, *et al.*, Rev. Sci. Instrum. **61**, 3552 (1990).

[3] E.J. Strait, *et al.*, Phys. Rev. Lett. **75**, 4421 (1995).

[4] F.M. Levinton, *et al.*, Phys. Rev. Lett. **75**, 4417 (1995).

[5] T. Fujita, *et al.*, Phys. Rev. Lett. **78**, 2377 (1997).

[6] K.H. Burrell, Phys. Plasmas **4**, 1499 (1997).

[7] B.W. Rice, *et al.*, Nucl. Fusion **37**, 517 (1997).

[8] M.C. Zarnstorff, *et al.*, Phys. Plasmas **4**, 1097 (1997).

[9] B.W. Rice, *et al.*, Phys. Rev. Lett. **79**, 2694 (1997).

[10] D. Wroblewski and L.L. Lao, Rev. Sci. Instrum. **63**, 5140 (1992).

[11] B.W. Rice, D.G. Nilson, D. Wroblewski, Rev. Sci. Instrum. **66**, 373 (1995).

[12] L.L. Lao, *et al.*, Nucl. Fusion **30**, 1035 (1990).

[13] P. Gohil, *et al.*, in *Proc. 14th IEEE/NPSS Symposium on Fusion Technology*, Vol. II, 1199 (1992).

[14] B.W. Rice, *et al.* Plasma Phys. Control. Fusion **38**, 869 (1996).
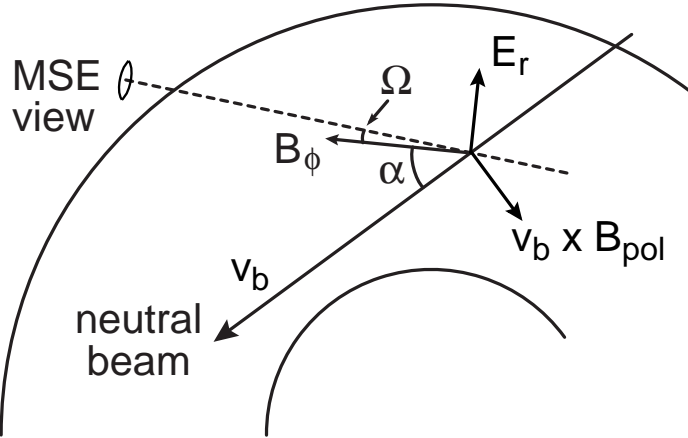
FIG. 1. MSE viewing geometry, indicating both the radial electric field, E_r, and the $v \times B_{pol}$ component of the Lorentz field.
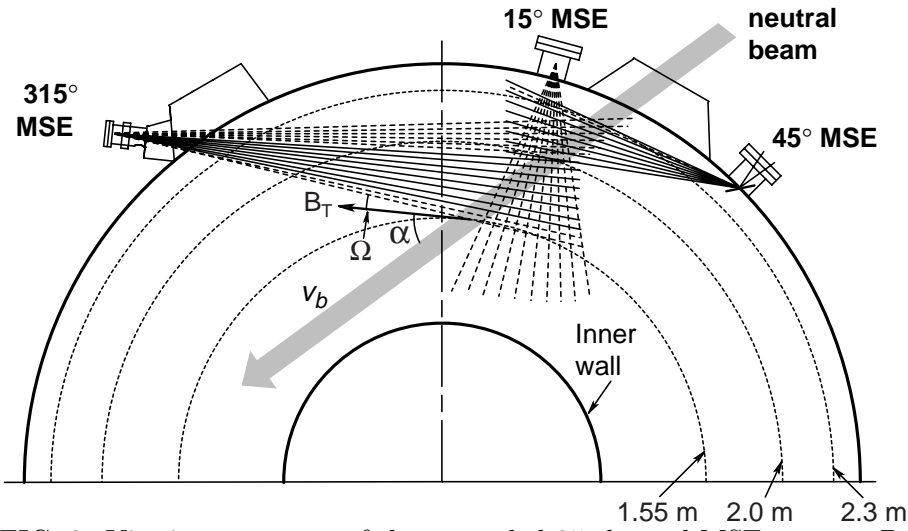
FIG. 2. Viewing geometry of the upgraded 35 channel MSE system. Dashed lines indicate the new chords added to determine E_r.
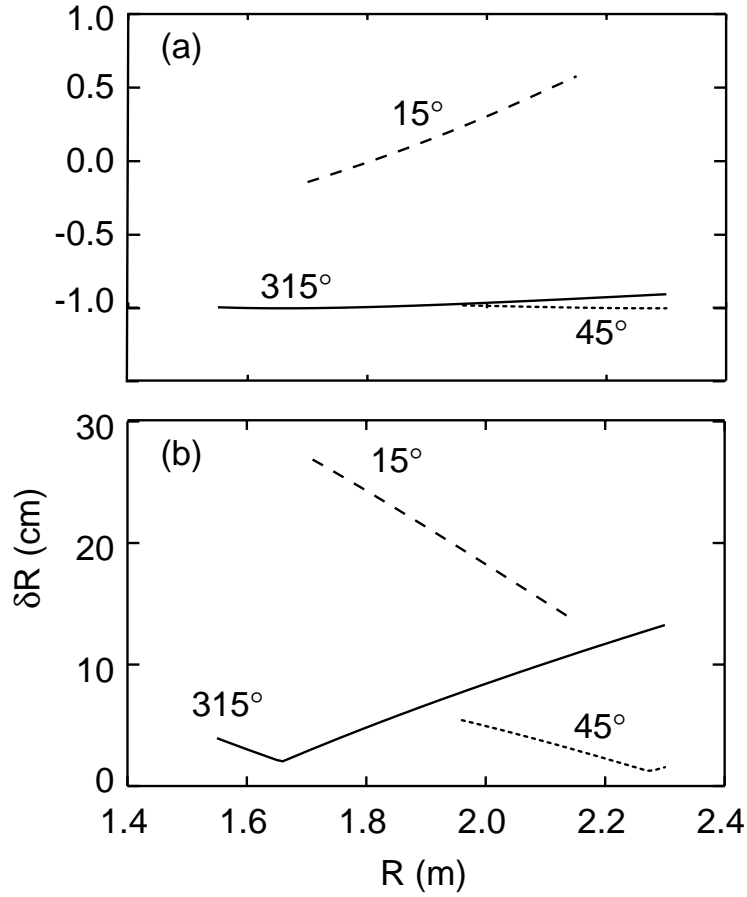
FIG. 3. Radial variation of the (a) A_5 coefficient and (b) spatial resolution for the three MSE viewports.
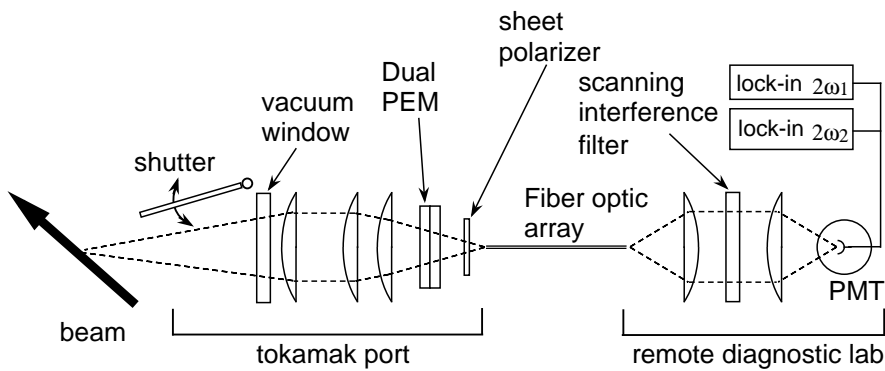
FIG. 4. Overview of the instrument design for the new radial viewing MSE system.
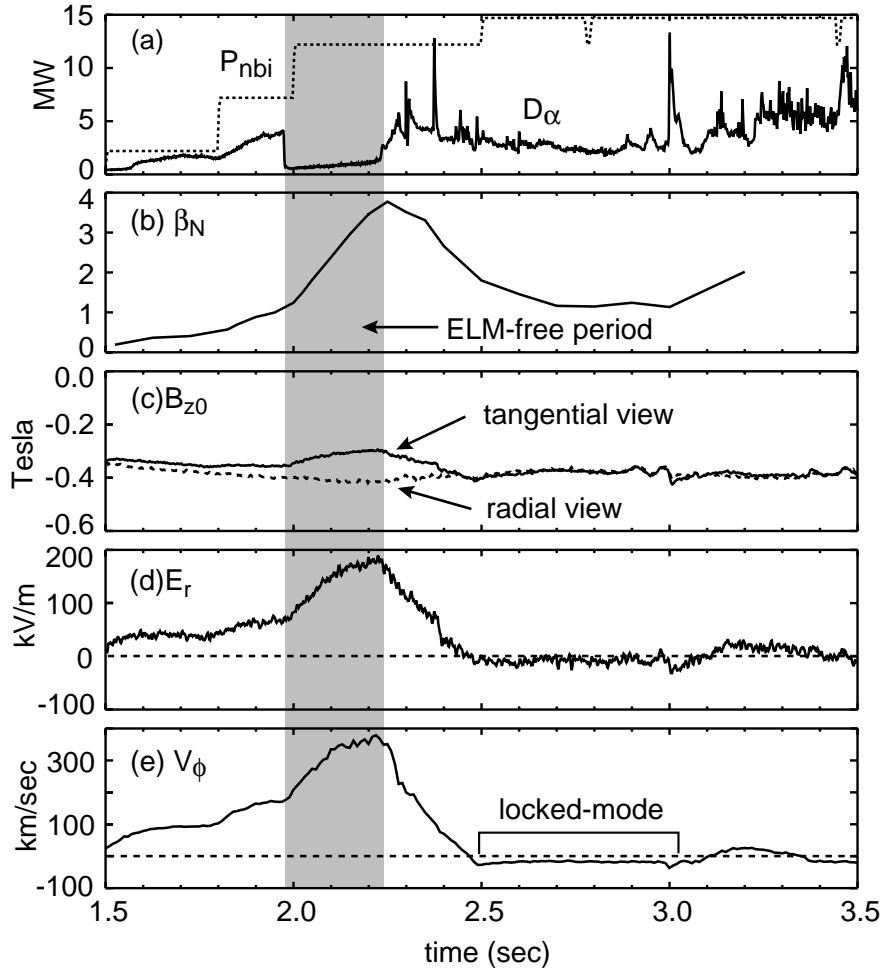
FIG. 5. Time evolution of discharge 92043: (a) neutral beam power and D_α emission, (b) normalized beta, (c) MSE B_{Z0} measurement at $R = 2$ m, (d) local value of E_r calculated from the data in (c) using Eq. (4), (e) CER toroidal rotation at $R = 1.9$ m.
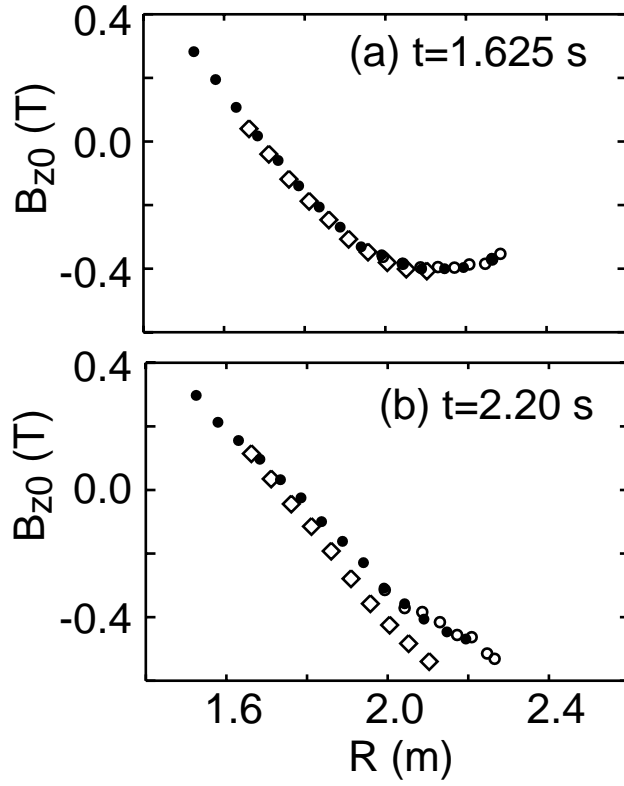
FIG. 6. Profiles of MSE B_{Z0} measurements for two phases of discharge 92043: (a) Low-power L-mode phase with low plasma rotation and E_r field; (b) high-performance phase with peak $E_r \sim 170$ kV/m. Circles are tangential chords and diamonds are radial chords.
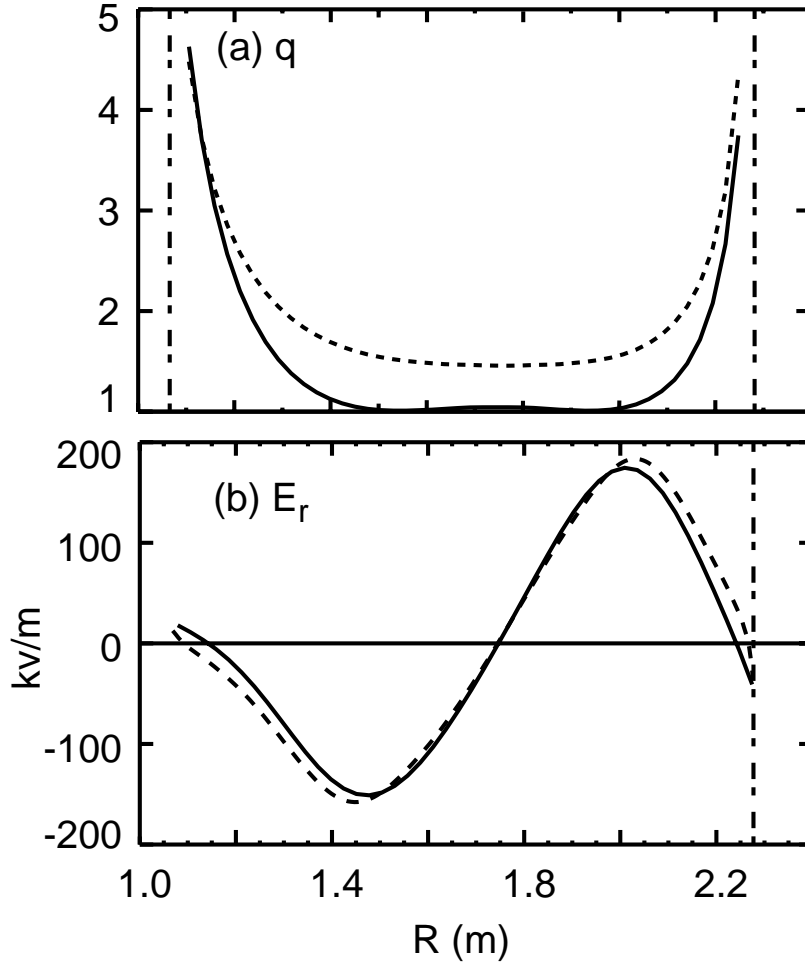
FIG. 7. EFIT equilibrium reconstruction including E_r for 92043 at 2.2 s: (a) q profile obtained using all MSE chords and including E_r (solid line) versus that obtained using only tangential MSE chords and assuming $E_r = 0$ (dashed line); (b) E_r determined from EFIT (solid line) and CER analysis of carbon impurities (dashed line).
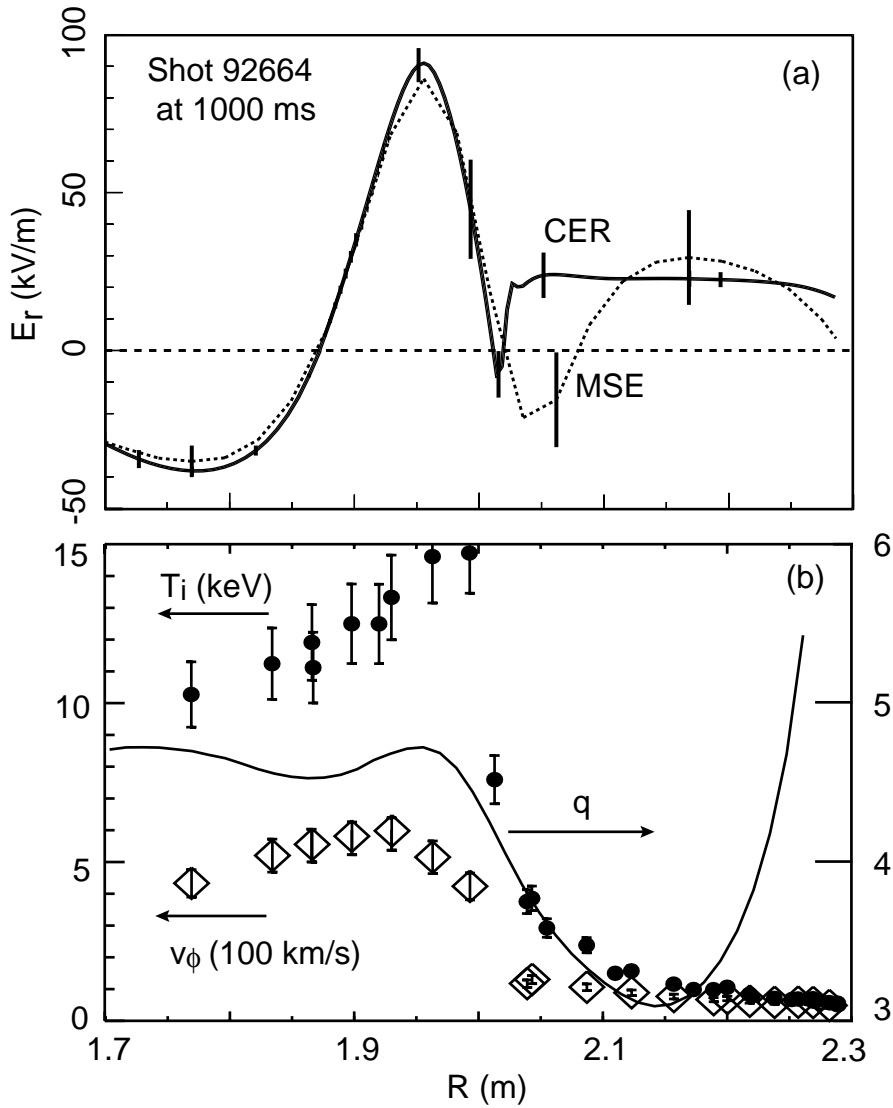
FIG. 8. (a) E_r profile for NCS discharge 92664 from MSE measurements (dashed) and CER measurements (solid); (b) profiles of T_i, toroidal rotation, v_ϕ, and q, indicating the steep internal transport barrier at $R = 2$ ms.
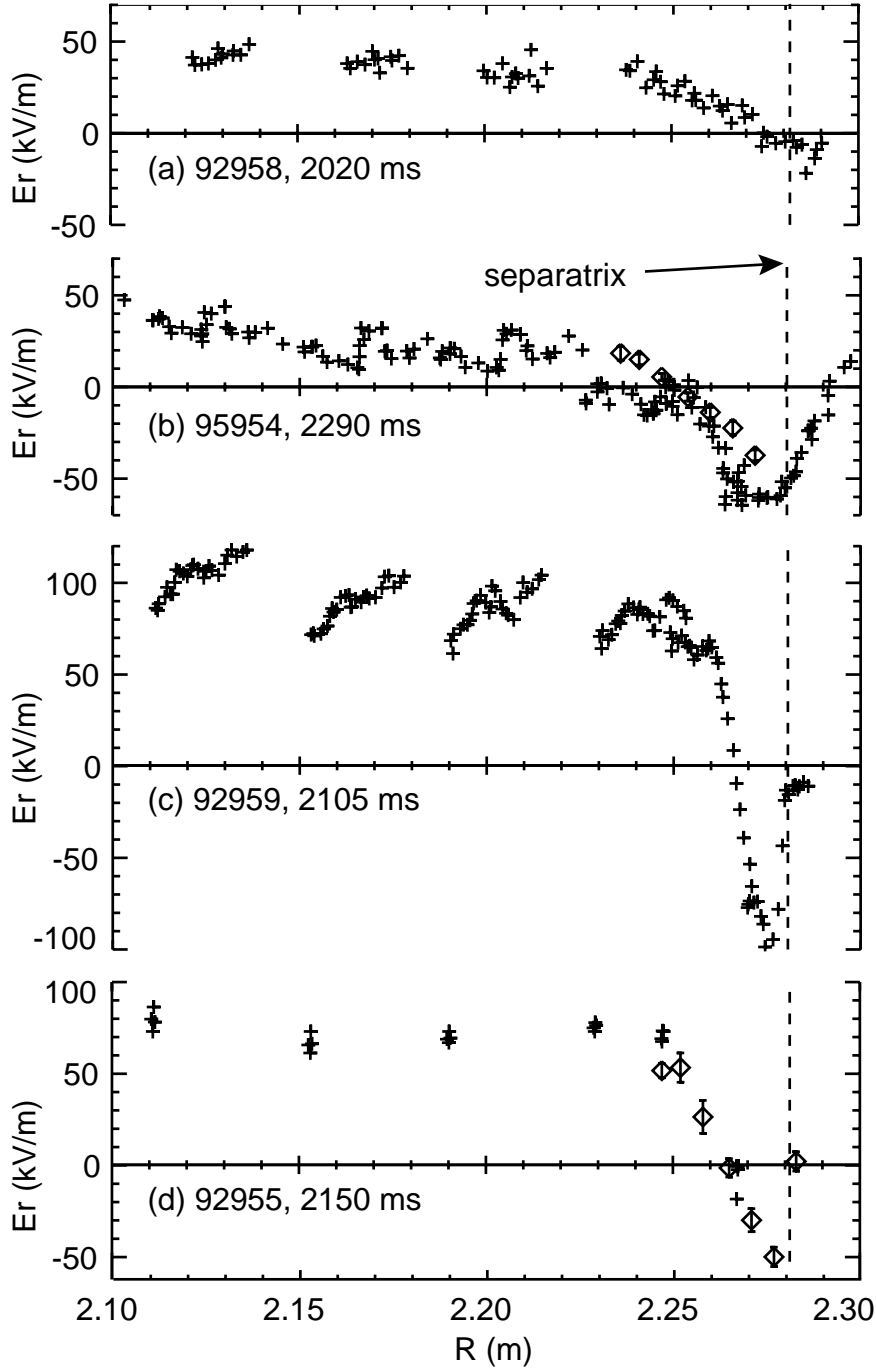
FIG. 9. MSE E_r profiles (plus symbols) for (a) L-mode , (b) ELMing H-mode and (c) ELM-free VH-mode during a separatrix sweep. CER measurements (diamonds) are shown for comparison in (b). In (d), a comparison between CER and MSE measurements is shown for a discharge that did not have a separatrix sweep.

19
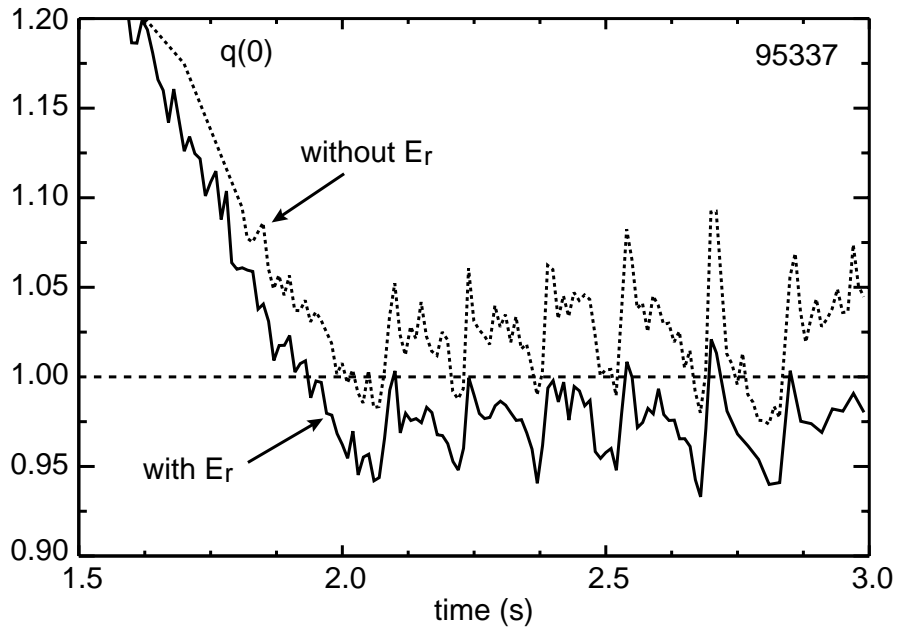
FIG. 10. Value of q_0 during a sawtoothing discharge determined from MSE data without E_r correction (dashed) and with E_r correction (solid).